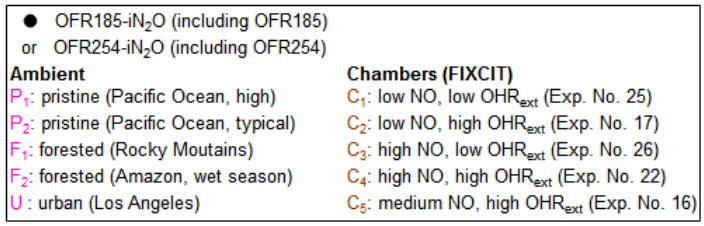

13

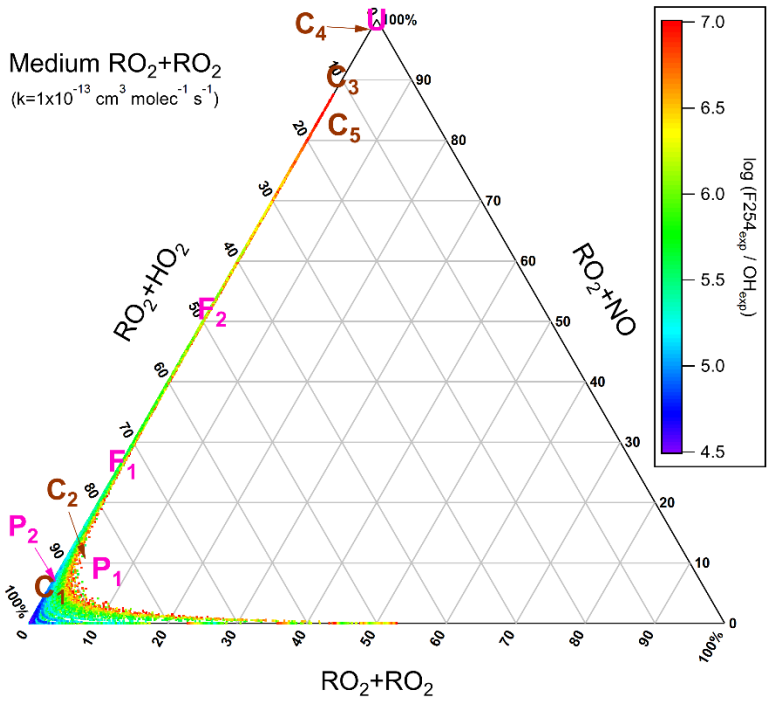

14

15 **(a) OFR254-7, medium RO_2+RO_2**

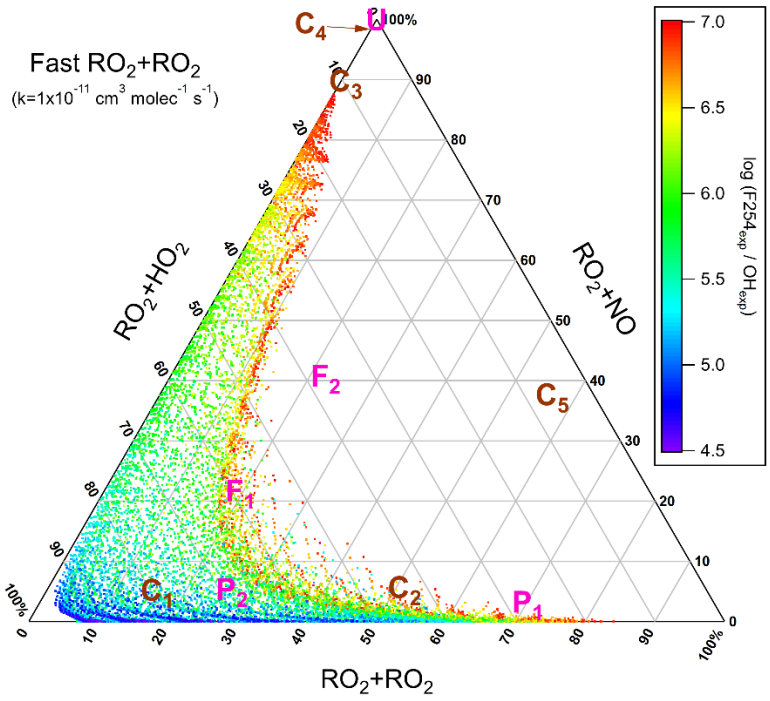

16

17 **(b) OFR254-7, fast RO_2+RO_2**

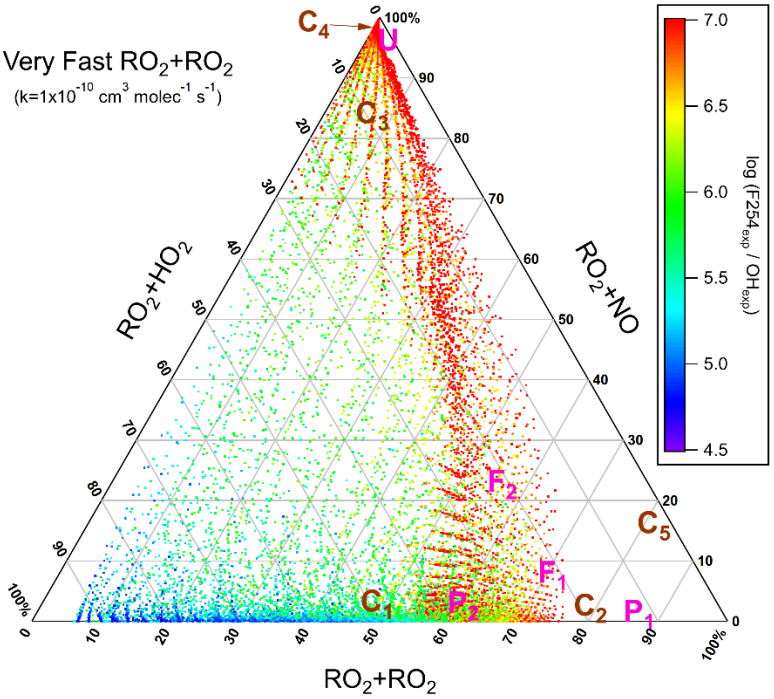

(c) OFR185, very fast RO_2+RO_2

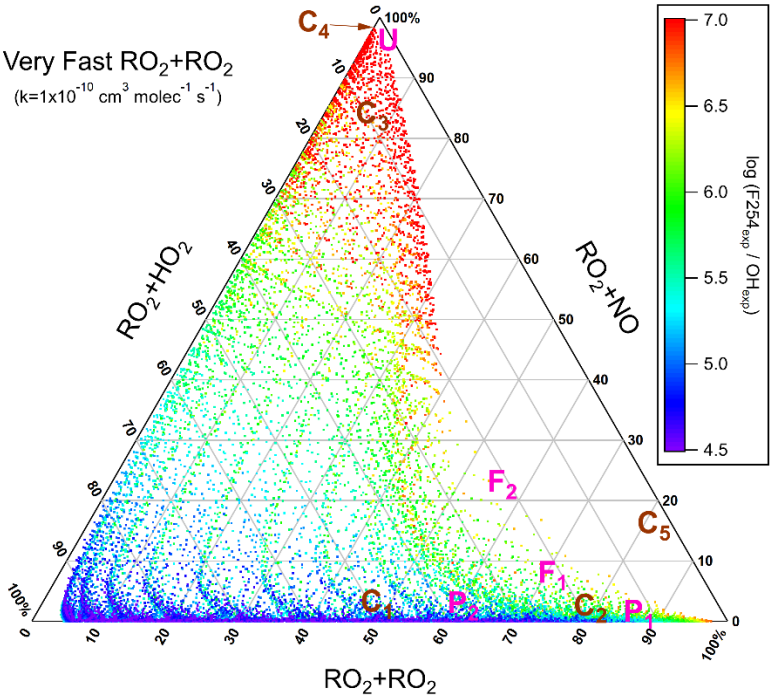

(d) OFR254-70, very fast RO_2+RO_2

Figure S1. Same format as Fig. 1, but for (a) medium and (b) fast RO_2+RO_2 in OFR254-7 (including OFR254-7-iN_2O) and very fast RO_2+RO_2 in (c) OFR185 (including OFR185-iN_2O) and (d) OFR254-70 (including OFR254-70-iN_2O).

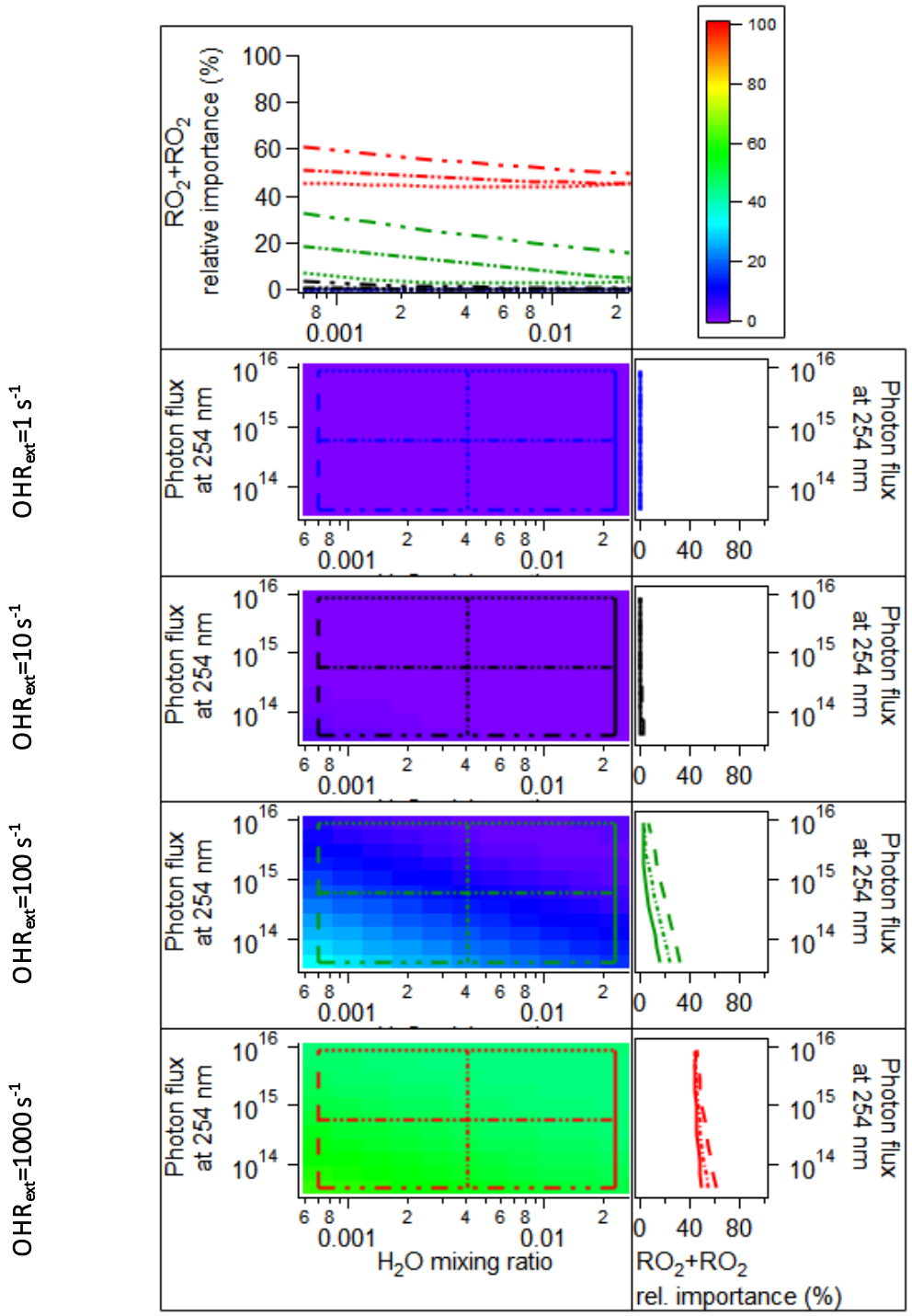

Figure S2. Dependence of the relative importance of RO_2+RO_2 in the fate of RO_2 (with the medium self/cross reaction rate constant and without RO_2+OH and RO_2 isomerization considered) on H_2O and UV, for OHR_{ext} of 1, 10, 100, and 1000 s^{-1} (first, second, third, and fourth row of image plots in each multi-panel composite, respectively) in OFR254-70 (N_2O=0). The panels above and on the right of image plots are the line plots of the RO_2+RO_2 relative importance in several typical cases. These cases are denoted in the image plots by horizontal or vertical lines of the same color and pattern as in the line plots. The cut lines are in blue, black, dark green, and red in the plots for the cases at different external OH reactivity (excluding NO_y) levels.

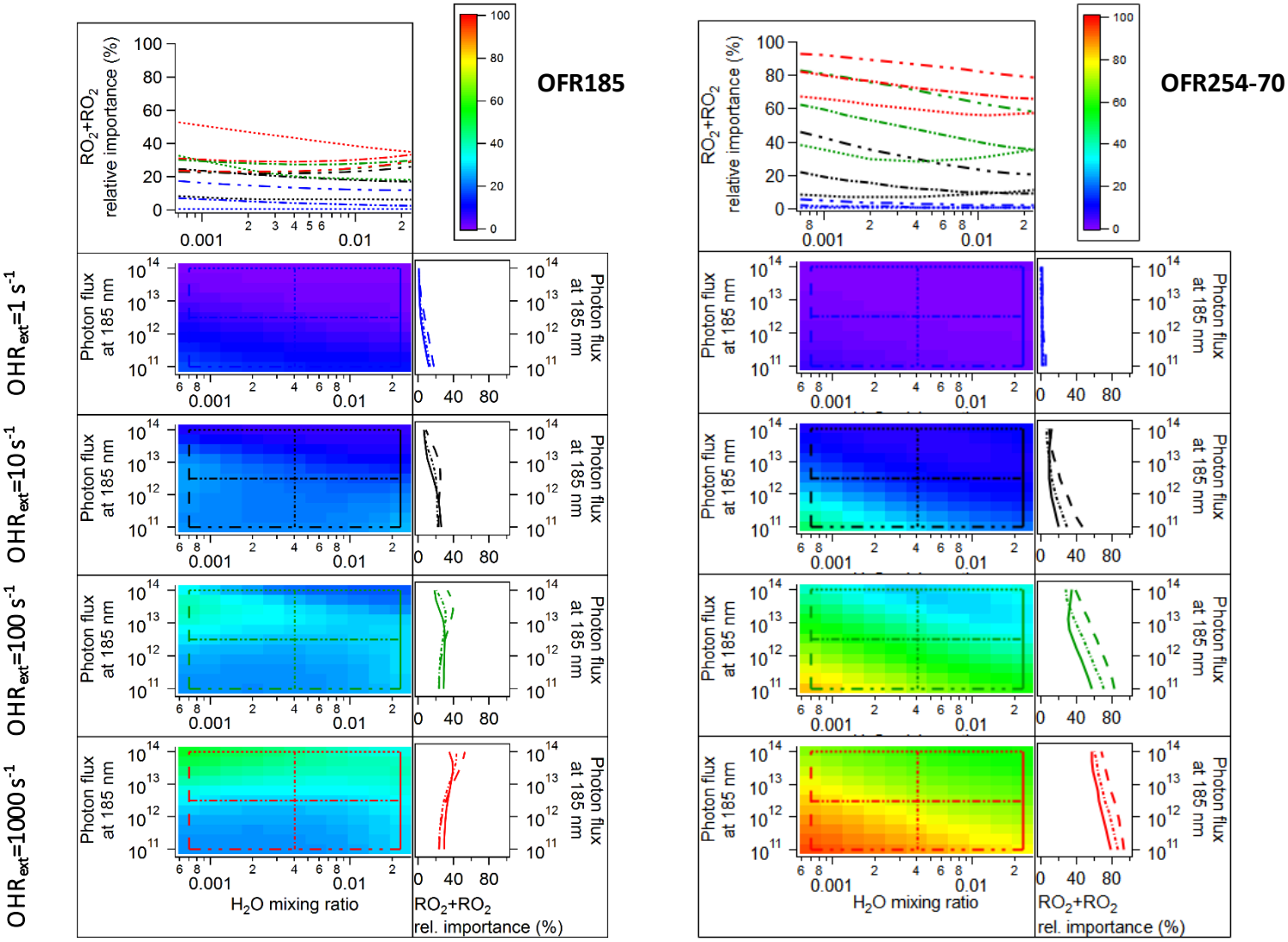
OFR185
OFR254-70
OHR$_{ext}$=1000 s^{-1}
OHR$_{ext}$=100 s^{-1}
OHR$_{ext}$=10 s^{-1}
OHR$_{ext}$=1 s^{-1}
RO$_2$+RO$_2$ relative importance (%)
Photon flux at 185 nm
H$_2$O mixing ratio
RO$_2$+RO$_2$ rel. importance (%)

Figure S3. Same format as Fig. S2, but for RO_2 with the fast self/cross reaction rate constants in OFR185 and OFR254-70 (N_2O=0).

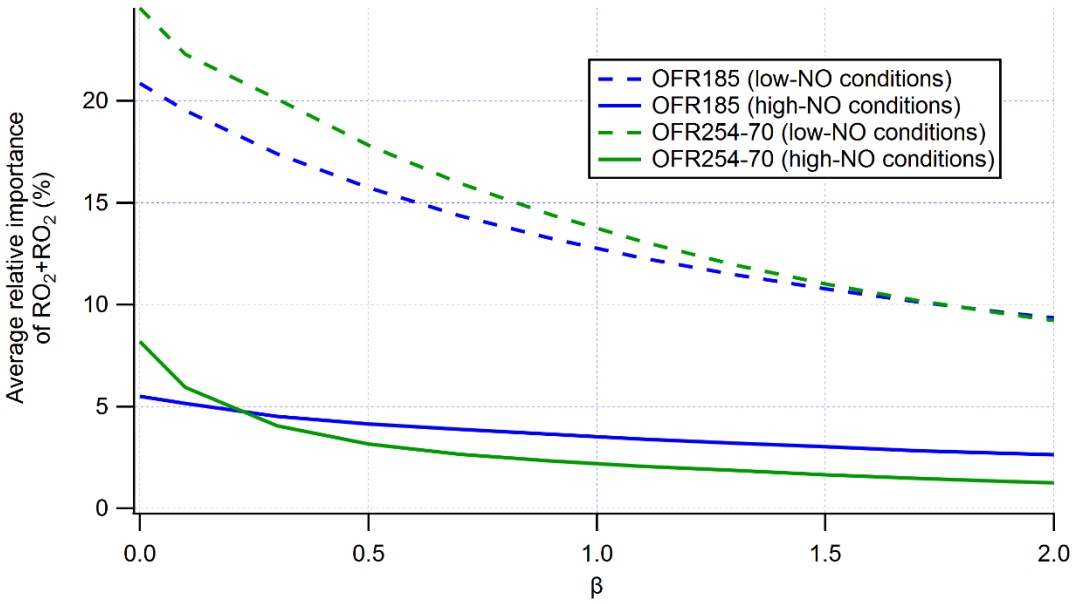

Figure S4. Average relative importance of RO_2+RO_2 in RO_2 fate (with fast self-/cross-reaction rate constant and without RO_2+OH and RO_2 isomerization considered) for OFR185 (including OFR185-iN_2O) and OFR254-70 (including OFR254-70-iN_2O) high-/low-NO conditions as a function of HO_x recycling ratio (β, see Section 2.3 for its definition) in a sensitivity study with a fixed β for each of the sensitivity cases.

45

● OFR185-iN_2O (including OFR185)
or OFR254-iN_2O (including OFR254)

Ambient	**Chambers (FIXCIT)**
P_1: pristine (Pacific Ocean, high)	C_1: low NO, low OHR_{ext} (Exp. No. 25)
P_2: pristine (Pacific Ocean, typical)	C_2: low NO, high OHR_{ext} (Exp. No. 17)
F_1: forested (Rocky Moutains)	C_3: high NO, low OHR_{ext} (Exp. No. 26)
F_2: forested (Amazon, wet season)	C_4: high NO, high OHR_{ext} (Exp. No. 22)
U : urban (Los Angeles)	C_5: medium NO, high OHR_{ext} (Exp. No. 16)

46

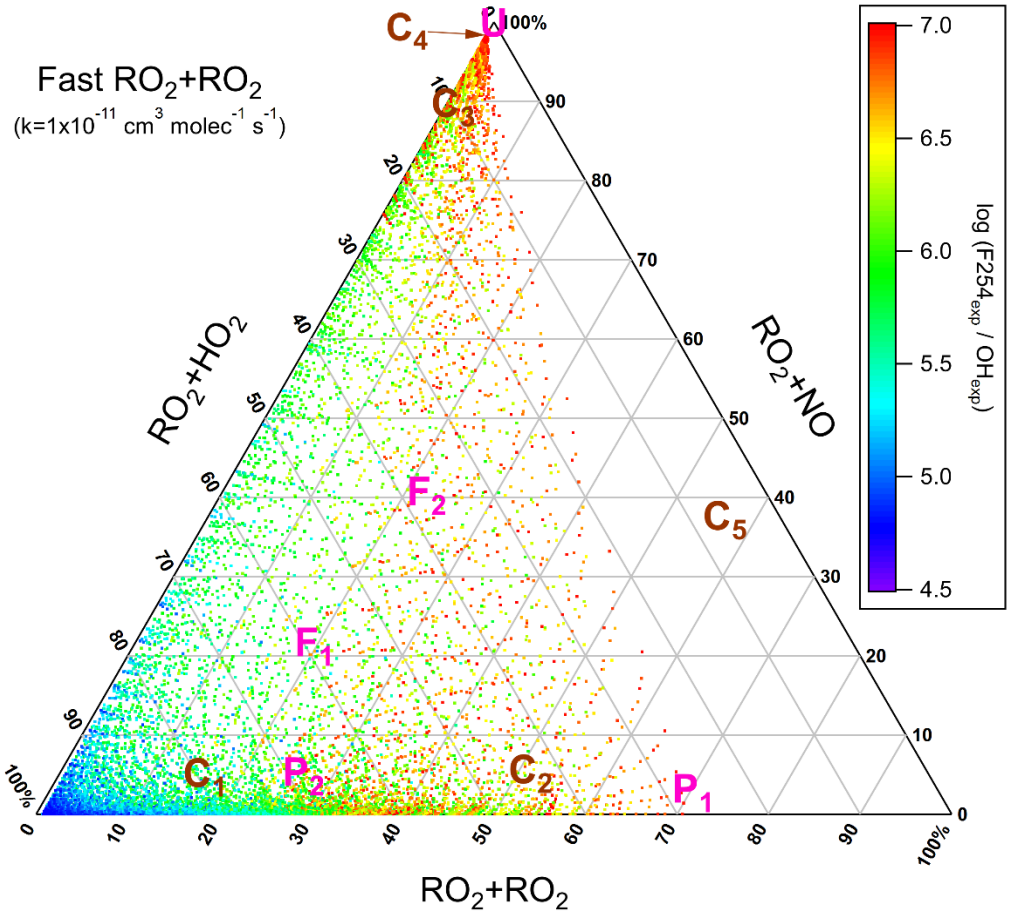

47

48 **(a) OFR185 (β=0)**

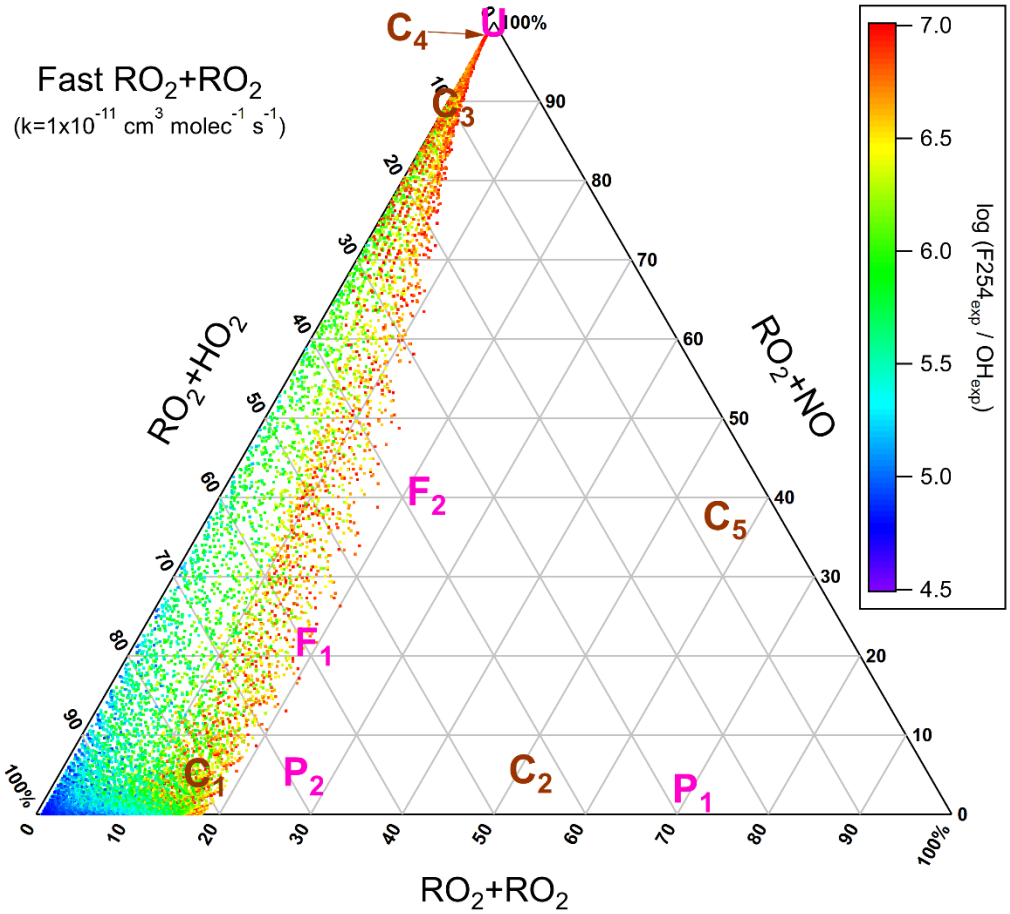
Fast RO2+RO2
(k=1x10-11 cm3 molec-1 s-1)
C4
C3
F2
C5
F1
C1
P2
C2
P1
RO2+HO2
RO2+NO
RO2+RO2
log (F254exp / OHexp)
7.0
6.5
6.0
5.5
5.0
4.5

(b) OFR185 (β=2)

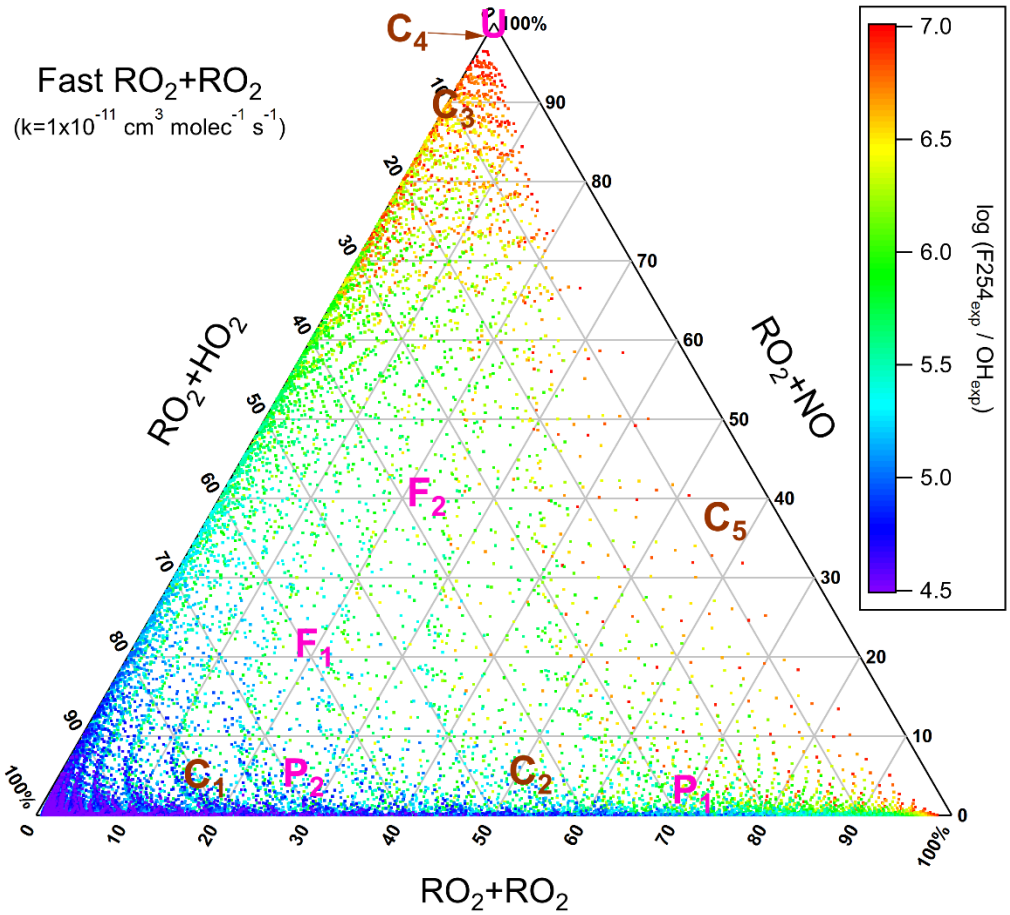

51
52 **(c) OFR254-70 (β=0)**

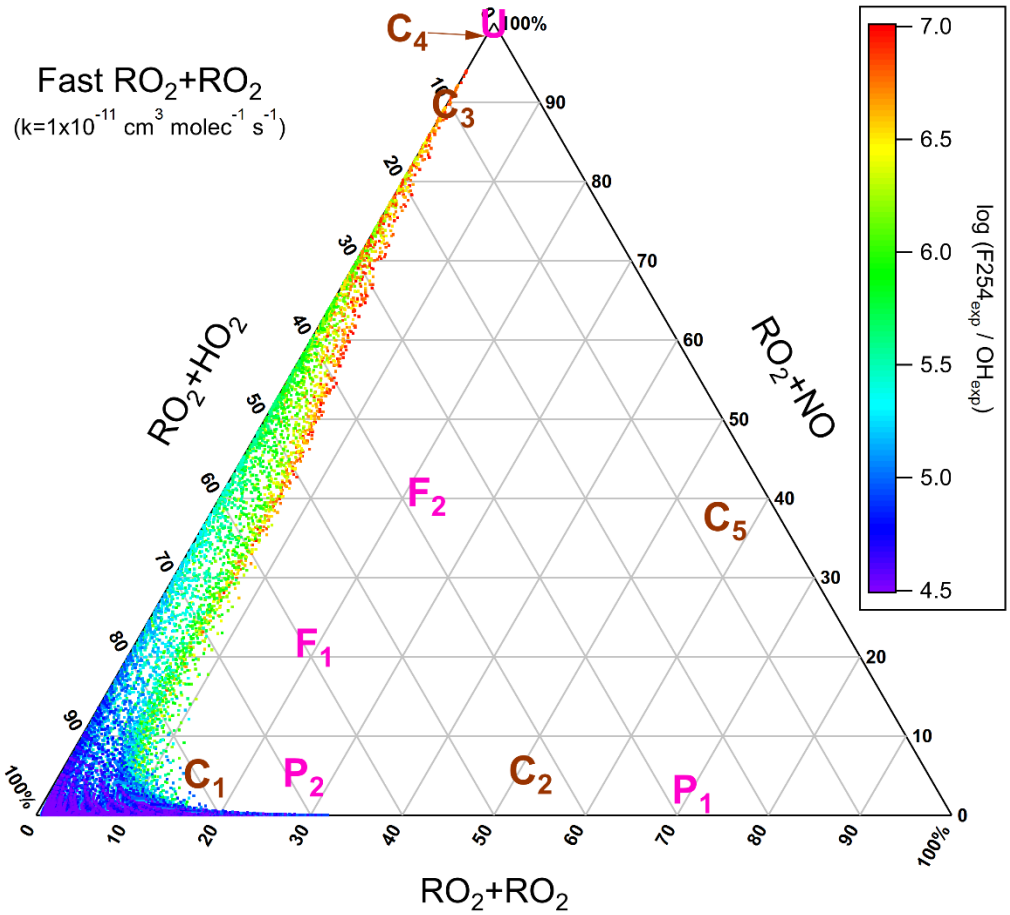

Figure S5. Same format as Fig. 1, but for sensitivity cases with fixed HO_x recycling ratio (β).

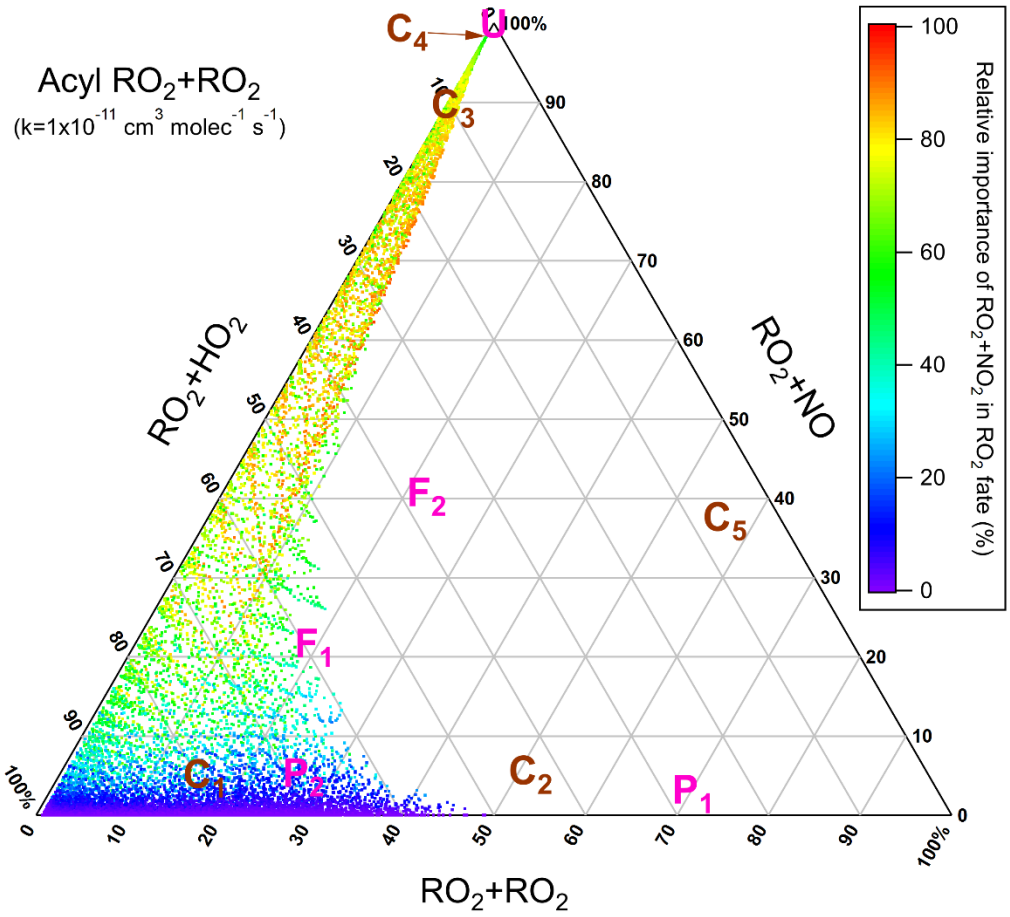

57
58

(a) OFR185

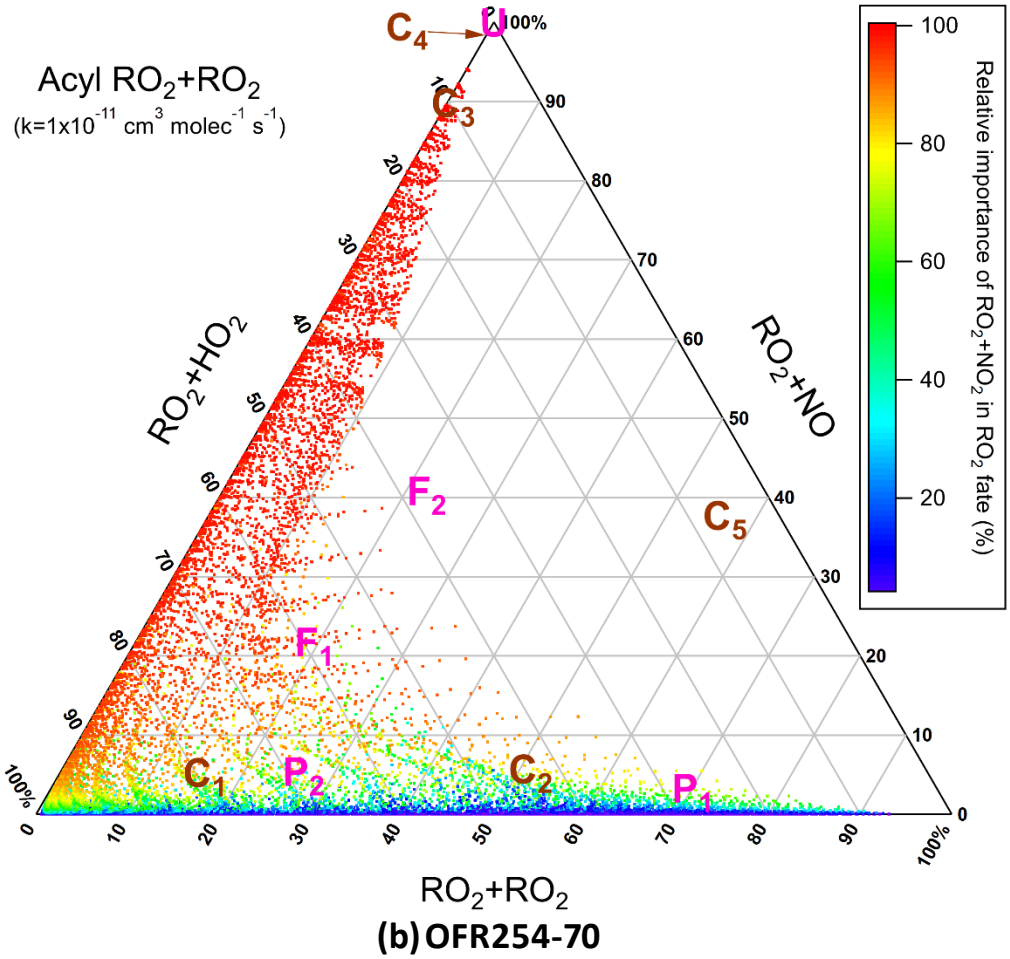

Figure S6. Same format as Fig. 1, but for acyl RO_2 (without RO_2+OH and RO_2 isomerization considered) in OFR185 (including OFR185-iN_2O), OFR254-70 (including OFR254-70-iN_2O). Note that the triangle plots in this figure only show the relative contributions of RO_2+HO_2, RO_2+NO and RO_2+RO_2 to their sum, not to the total loss of acyl RO_2.

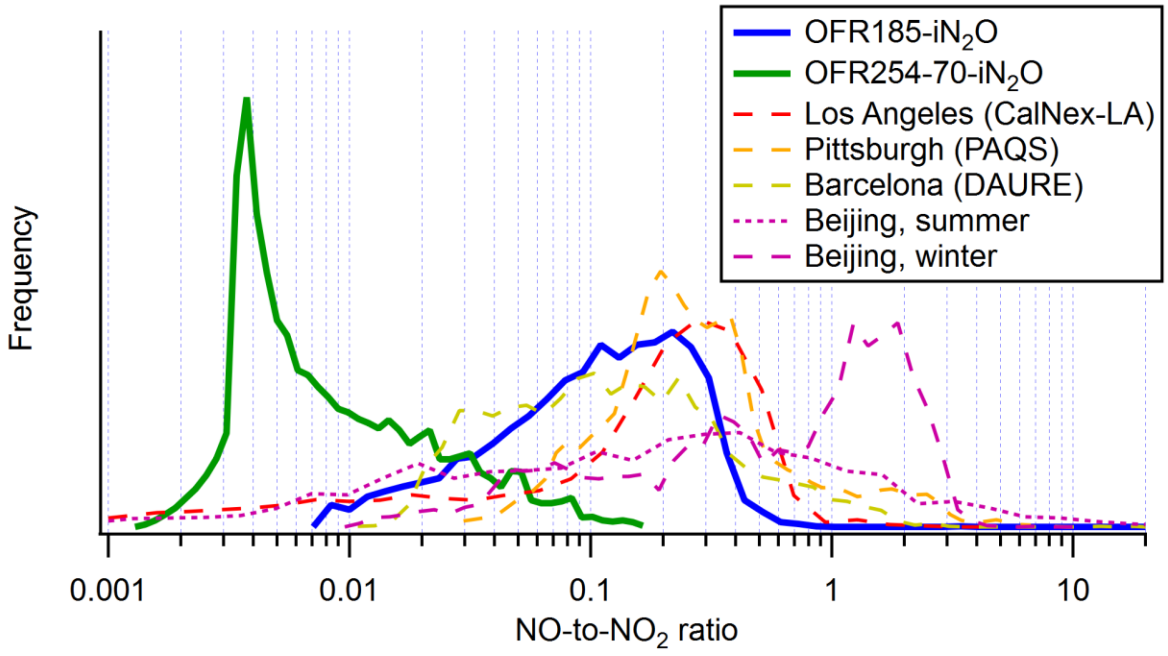

66

67 **Figure S7.** Frequency occurrence distributions of NO-to-NO_2 ratios for OFR185-iN_2O and OFR254-70-
68 iN_2O model cases and measured at the Los Angeles, Pittsburgh and Barcelona ground sites during the
69 CalNex-LA 2010, PAQS 2002 and DAURE 2009 campaigns, respectively (Zhang et al., 2005; Reche et al.,
70 2011; Ryerson et al., 2013) and at a ground site in Beijing in both summer and winter (Hu et al., 2016).
71 OFR cases under bad conditions are filtered out. The total areas of all distributions are identical.

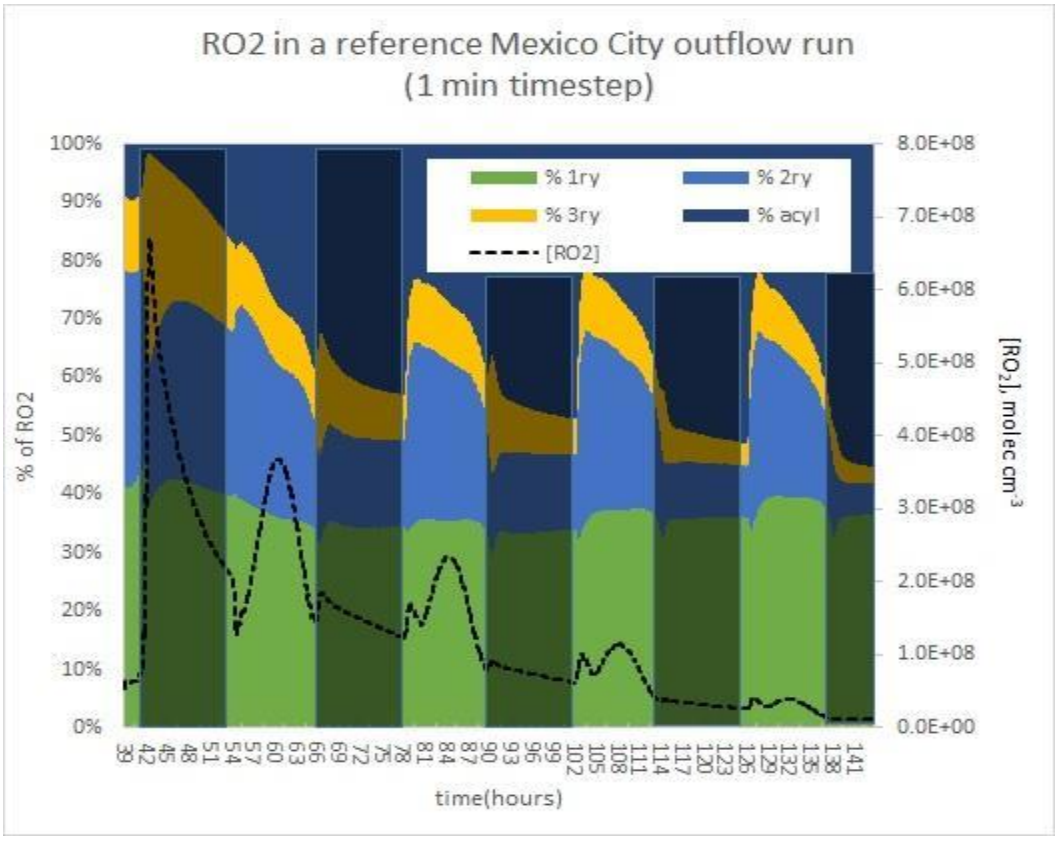
RO2 in a reference Mexico City outflow run
(1 min timestep)
% of RO2
[RO2], molec cm-3
time(hours)
% 1ry
% 2ry
% 3ry
% acyl
[RO2]

72

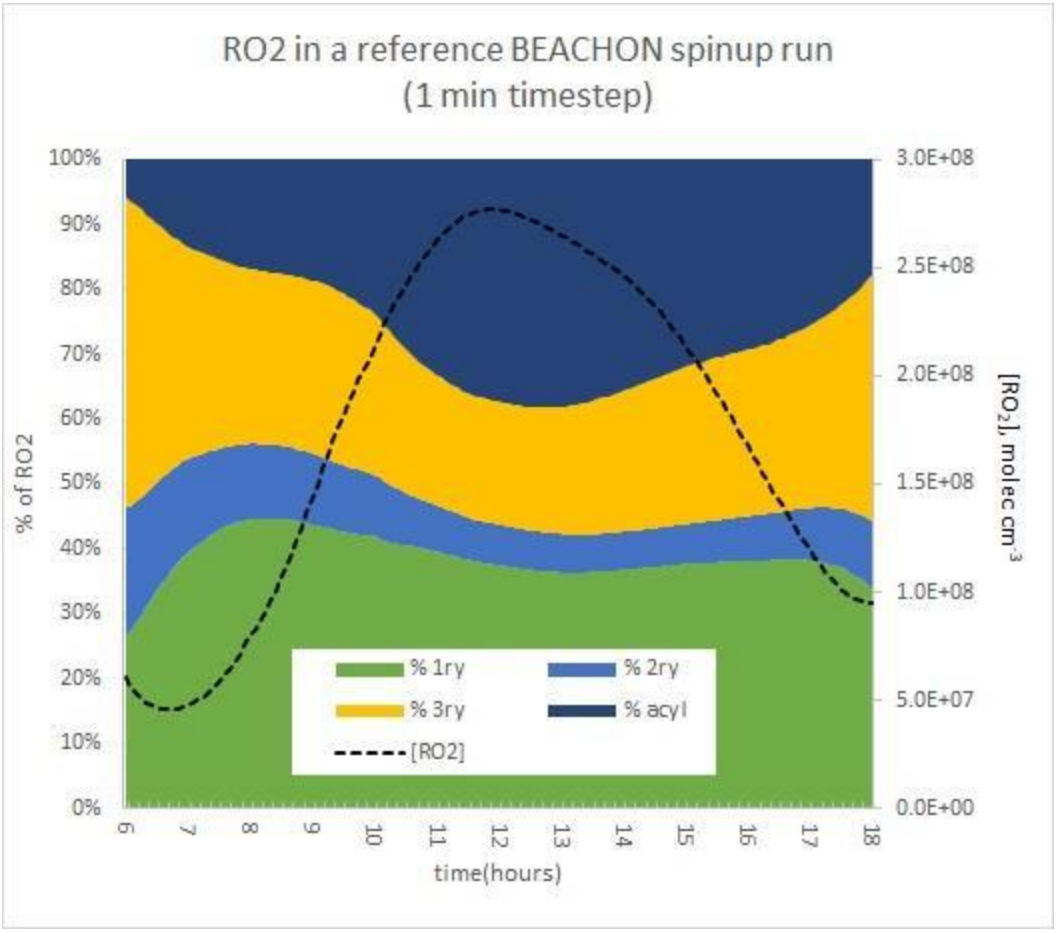
RO2 in a reference BEACHON spinup run
(1 min timestep)
% of RO2
[RO2], molec cm-3
time(hours)
% 1ry
% 2ry
% 3ry
% acyl
[RO2]

73

Figure S8. (a) RO_2 concentration and composition [primary (1ry), secondary (2ry), tertiary (3ry) and acyl RO_2] as a function of aging time for the simulation of a parcel of air advected from Mexico City during the MILAGRO 2006 campaign using the fully explicit GECKO-A model (Lee-Taylor et al., 2015). (b) The same for a GECKO-A simulation of air in a Rocky Mountain pine forest for the average diurnal cycle during the BEACHON-RoMBAS 2011 campaign (Palm et al., 2016; Hunter et al., 2017). Nighttime is denoted by shaded area.

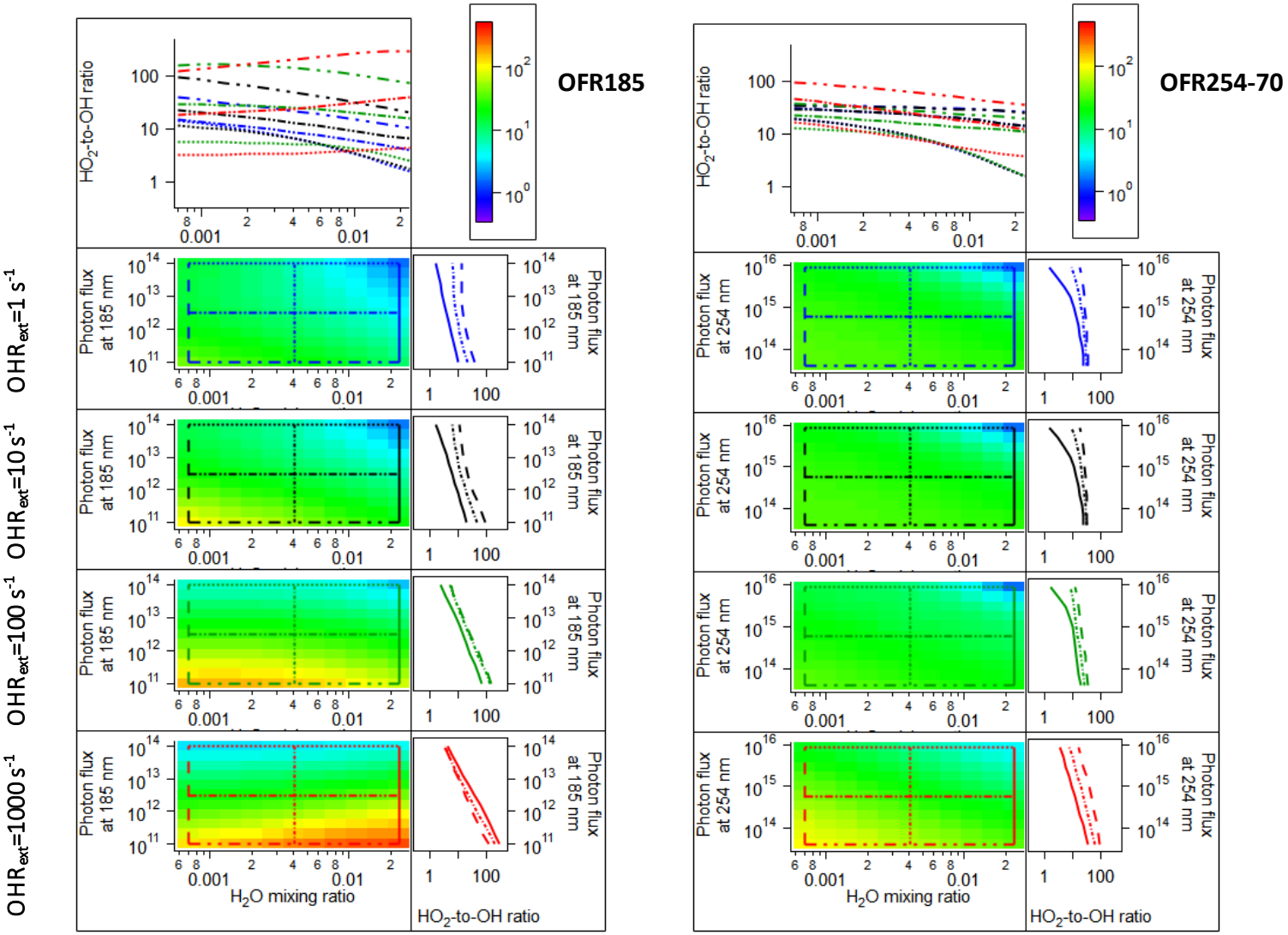

Figure S9. Same format as Fig. S3, but for the HO_2-to-OH ratio in OFR185 and OFR254-70 (N_2O=0) cases with medium RO_2 self/cross reaction rate constant.

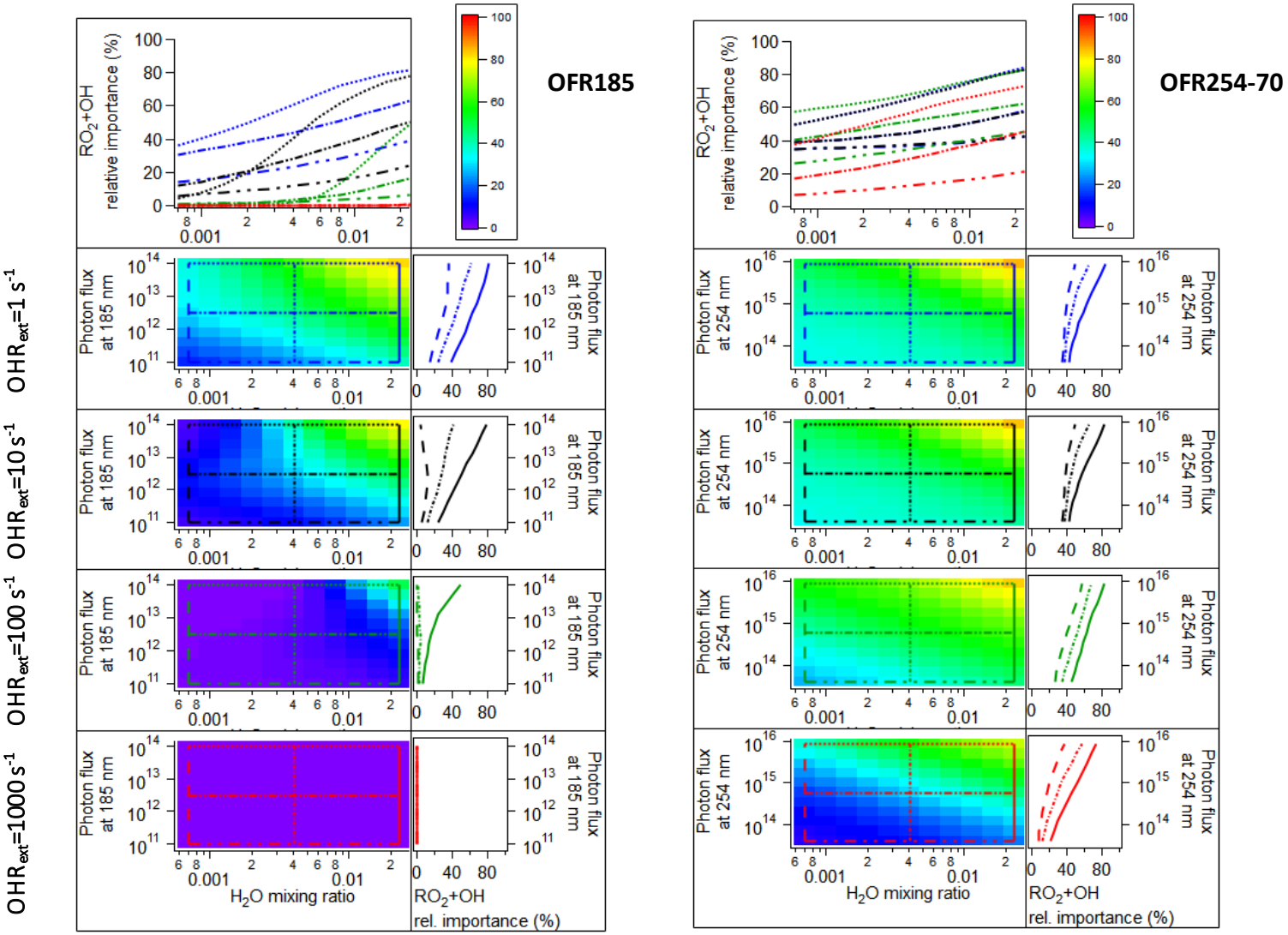

Figure S10. Same format as Fig. S3, but for the relative importance of RO_2+OH in the fate of RO_2 (with medium RO_2 self/cross reaction rate constant) in OFR185 and OFR254-70 (N_2O=0).

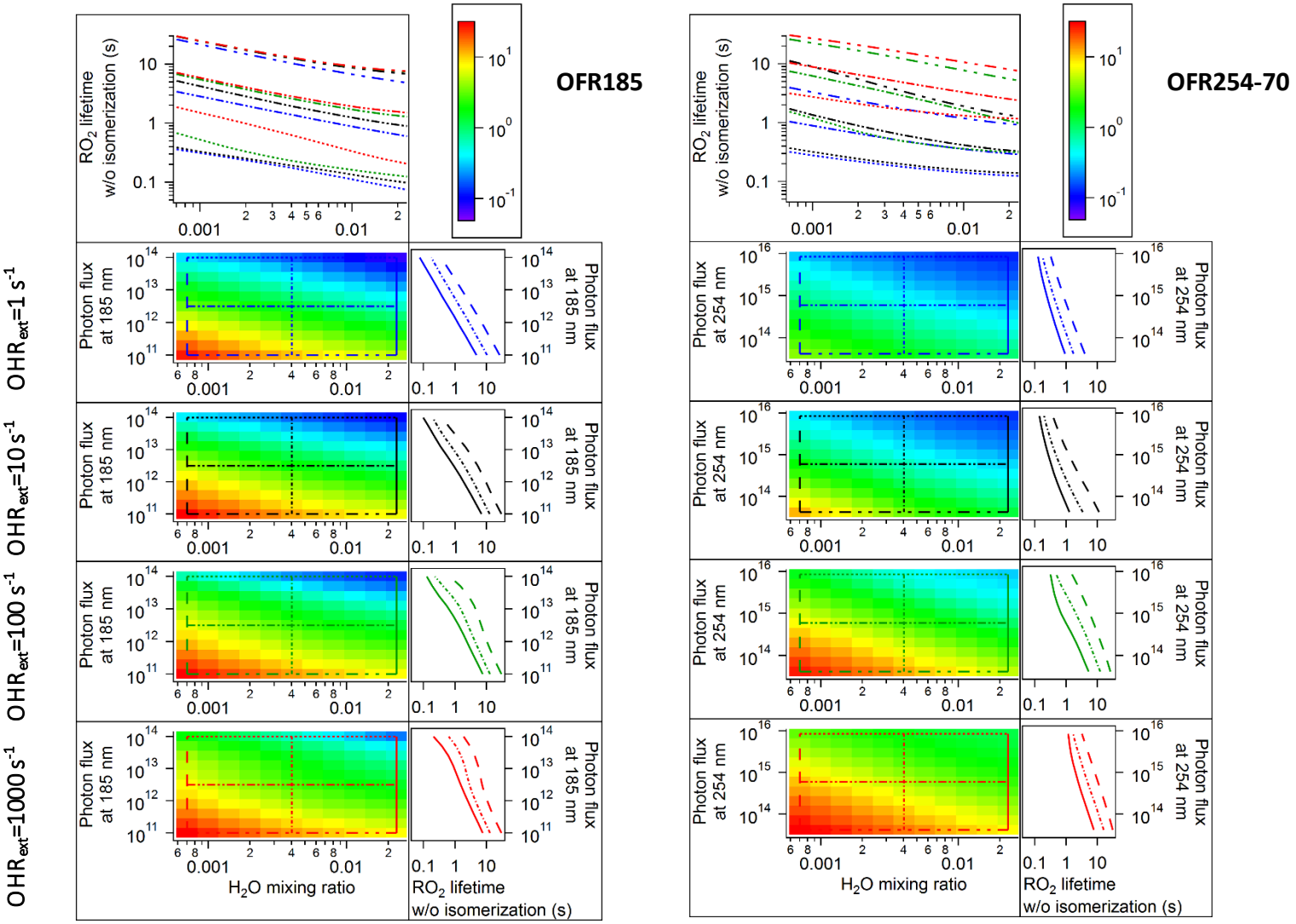

Figure S11. Same format as Fig. S3, but for the RO_2 lifetime [with medium RO_2 self/cross reaction rate constant and excluding the contribution of RO_2 isomerization to its lifetime (but RO_2 isomerization included in the model)] in OFR185 and OFR254-70 (N_2O=0).

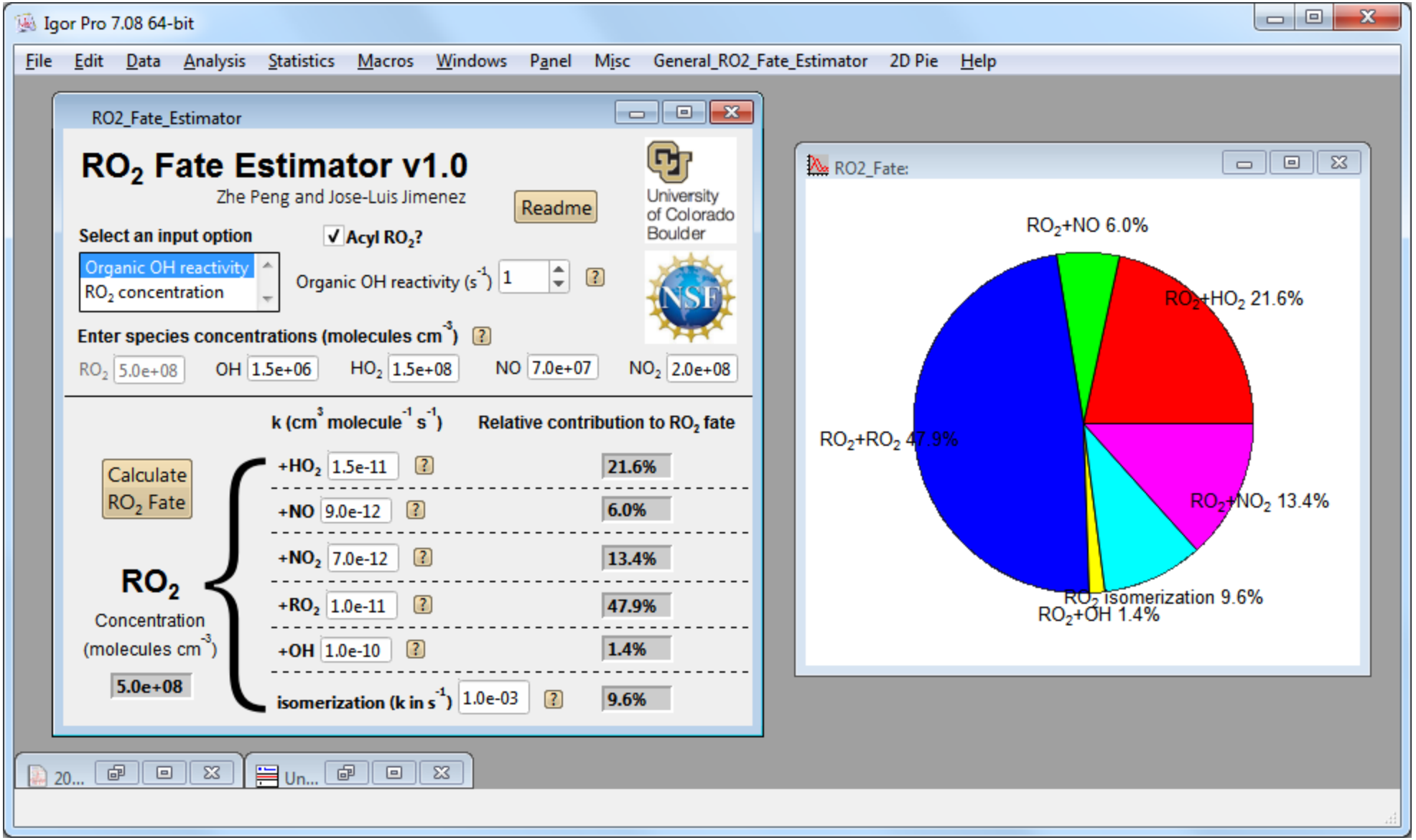

Figure S7. Screenshot of the layout of the General RO_2 Fate Estimator. The Estimator is running in Igor Pro v7 (WaveMetrics, Inc., Lake Oswego, Oregon, USA), which is downloadable at https://www.wavemetrics.com/software/igor-pro-708-installer.

Table S1. Definition of OFR condition types in this study (good/risky/bad high/low-NO). Good/risky/bad conditions are classified only in terms of non-tropospheric organic photolysis and this classification does *not* indicate whether RO_2 chemistry is atmospherically relevant.

Condition	Good	Risky	Bad
Criterion	$F185_{exp}/OH_{exp}<3x10^3$ cm s^{-1} and $F254_{exp}/OH_{exp}<4x10^5$ cm s^{-1}	$F185_{exp}/OH_{exp}<1x10^5$ cm s^{-1} and $F254_{exp}/OH_{exp}<1x10^7$ cm s^{-1} (excluding good conditions)	$F185_{exp}/OH_{exp}\geq1x10^5$ cm s^{-1} or $F254_{exp}/OH_{exp}\geq1x10^7$ cm s^{-1}

Condition	High-NO	Low-NO
Criterion	$\frac{r(RO_2+NO)}{r(RO_2+HO_2)} > 1$	$\frac{r(RO_2+NO)}{r(RO_2+HO_2)} \leq 1$

References

Hu, W., Hu, M., Hu, W., Jimenez, J. L., Yuan, B., Chen, W., Wang, M., Wu, Y., Chen, C., Wang, Z., Peng, J., Zeng, L. and Shao, M.: Chemical composition, sources, and aging process of submicron aerosols in Beijing: Contrast between summer and winter, J. Geophys. Res. Atmos., 121(4), 1955–1977, doi:10.1002/2015JD024020, 2016.

Hunter, J. F., Day, D. A., Palm, B. B., Yatavelli, R. L. N., Chan, A. W. H., Kaser, L., Cappellin, L., Hayes, P. L., Cross, E. S., Carrasquillo, A. J., Campuzano-Jost, P., Stark, H., Zhao, Y., Hohaus, T., Smith, J. N., Hansel, A., Karl, T., Goldstein, A. H., Guenther, A., Worsnop, D. R., Thornton, J. A., Heald, C. L., Jimenez, J. L. and Kroll, J. H.: Comprehensive characterization of atmospheric organic carbon at a forested site, Nat. Geosci., 10(10), 748–753, doi:10.1038/NGEO3018, 2017.

Lee-Taylor, J., Hodzic, A., Madronich, S., Aumont, B., Camredon, M. and Valorso, R.: Multiday production of condensing organic aerosol mass in urban and forest outflow, Atmos. Chem. Phys., 15(2), 595–615, doi:10.5194/acpd-14-17999-2014, 2015.

Palm, B. B., Campuzano-Jost, P., Ortega, A. M., Day, D. A., Kaser, L., Jud, W., Karl, T., Hansel, A., Hunter, J. F., Cross, E. S., Kroll, J. H., Peng, Z., Brune, W. H. and Jimenez, J. L.: In situ secondary organic aerosol formation from ambient pine forest air using an oxidation flow reactor, Atmos. Chem. Phys., 16(5), 2943–2970, doi:10.5194/acp-16-2943-2016, 2016.

Reche, C., Viana, M., Moreno, T., Querol, X., Alastuey, A., Pey, J., Pandolfi, M., Prévôt, A., Mohr, C., Richard, A., Artiñano, B., Gomez-Moreno, F. J. and Cots, N.: Peculiarities in atmospheric particle number and size-resolved speciation in an urban area in the western Mediterranean: Results from the DAURE campaign, Atmos. Environ., 45(30), 5282–5293, doi:10.1016/j.atmosenv.2011.06.059, 2011.

Ryerson, T. B., Andrews, A. E., Angevine, W. M., Bates, T. S., Brock, C. A., Cairns, B., Cohen, R. C., Cooper, O. R., De Gouw, J. A., Fehsenfeld, F. C., Ferrare, R. A., Fischer, M. L., Flagan, R. C., Goldstein, A. H., Hair, J. W., Hardesty, R. M., Hostetler, C. A., Jimenez, J. L., Langford, A. O., McCauley, E., McKeen, S. A., Molina, L. T., Nenes, A., Oltmans, S. J., Parrish, D. D., Pederson, J. R., Pierce, R. B., Prather, K., Quinn, P. K., Seinfeld, J. H., Senff, C. J., Sorooshian, A., Stutz, J., Surratt, J. D., Trainer, M., Volkamer, R., Williams, E. J. and Wofsy, S. C.: The 2010 California Research at the Nexus of Air Quality and Climate Change (CalNex) field study, J. Geophys. Res. Atmos., 118(11), 5830–5866, doi:10.1002/jgrd.50331, 2013.

Zhang, Q., Canagaratna, M. R., Jayne, J. T., Worsnop, D. R. and Jimenez, J.-L.: Time- and size-resolved chemical composition of submicron particles in Pittsburgh: Implications for aerosol sources and processes, J. Geophys. Res., 110(D7), D07S09, doi:10.1029/2004JD004649, 2005.